microorganisms

MDPI

Article

Identification of Causal Relationships between Gut Microbiota and Influenza a Virus Infection in Chinese by Mendelian Randomization

Qijun Liao [1,2,†], Fuxiang Wang [1,†], Wudi Zhou [1], Guancheng Liao [1], Haoyang Zhang [3], Yuelong Shu [1,4,*] and Yongkun Chen [5,*]

[1] School of Public Health (Shenzhen), Shenzhen Campus of Sun Yat-sen University, Shenzhen 518107, China; liaoqj@mail2.sysu.edu.cn (Q.L.); wangfx6@mail2.sysu.edu.cn (F.W.); zhouwd5@mail2.sysu.edu.cn (W.Z.); liaogch5@mail2.sysu.edu.cn (G.L.)
[2] BGI Genomics, Shenzhen 518085, China
[3] School of Data and Computer Science, Sun Yat-sen University, Guangzhou 510006, China; zhanghaoyang0@hotmail.com
[4] Key Laboratory of Pathogen Infection Prevention and Control (MOE), State Key Laboratory of Respiratory Health and Multimorbidity, National Institute of Pathogen Biology, Chinese Academy of Medical Sciences and Peking Union Medical College, Beijing 102629, China
[5] Guangdong Provincial Key Laboratory of Infection Immunity and Inflammation, Department of Pathogen Biology, School of Basic Medical Sciences, Shenzhen University Medical School, Shenzhen University, Shenzhen 518055, China
* Correspondence: shuylong@mail.sysu.edu.cn (Y.S.); chenyk@szu.edu.cn (Y.C.)
† These authors contributed equally to this work.

Abstract: Numerous studies have reported a correlation between gut microbiota and influenza A virus (IAV) infection and disease severity. However, the causal relationship between these factors remains inadequately explored. This investigation aimed to assess the influence of gut microbiota on susceptibility to human infection with H7N9 avian IAV and the severity of influenza A (H1N1)pdm09 infection. A two-sample Mendelian randomization analysis was conducted, integrating our in-house genome-wide association study (GWAS) on H7N9 susceptibility and H1N1pdm09 severity with a metagenomics GWAS dataset from a Chinese population. Twelve and fifteen gut microbiotas were causally associated with H7N9 susceptibility or H1N1pdm09 severity, separately. Notably, *Clostridium hylemonae* and *Faecalibacterium prausnitzii* were negative associated with H7N9 susceptibility and H1N1pdm09 severity, respectively. Moreover, *Streptococcus peroris* and *Streptococcus sanguinis* were associated with H7N9 susceptibility, while *Streptococcus parasanguini* and *Streptococcus suis* were correlated with H1N1pdm09 severity. These results provide novel insights into the interplay between gut microbiota and IAV pathogenesis as well as new clues for mechanism research regarding therapeutic interventions or IAV infections. Future studies should concentrate on clarifying the regulatory mechanisms of gut microbiota and developing efficacious approaches to reduce the incidence of IAV infections, which could improve strategy for preventing and treating IAV infection worldwide.

Keywords: H7N9; H1N1; influenza A virus; Mendelian randomization; microbiota

Citation: Liao, Q.; Wang, F.; Zhou, W.; Liao, G.; Zhang, H.; Shu, Y.; Chen, Y. Identification of Causal Relationships between Gut Microbiota and Influenza a Virus Infection in Chinese by Mendelian Randomization. *Microorganisms* **2024**, *12*, 1170. https://doi.org/10.3390/microorganisms12061170

Academic Editor: Denis Roy

Received: 17 May 2024
Revised: 1 June 2024
Accepted: 5 June 2024
Published: 8 June 2024

1. Introduction

Influenza A viruses (IAVs) are primarily transmitted among aquatic birds and poultry but can sporadically cross species barriers to infect humans. Certain subtypes, such as H1N1 and H3N2, are capable of adapting to humans, enabling person-to-person transmission and triggering pandemics. These strains may evolve into seasonal influenza viruses [1]. However, avian IAVs, such as H5N1 and H7N9, fail to fully adapt to humans, lacking efficient human-to-human transmission after spillover infection. Despite this, spillover events may result in a high case fatality rate and harbor the potential for a new pandemic if

the viruses continually evolve and adapt to humans [2]. According to the World Health Organization, seasonal IAV accounts for an estimated one billion infections, 3 to 5 million severe cases, and approximately 290,000 to 650,000 deaths each year [3]. Notably, avian IAV H7N9 triggered five outbreaks in China from 2013 to 2017, resulting in 1568 confirmed infections with a fatality rate of approximately 39%. To alleviate the public health impact of IAVs, it is imperative to investigate host factors influencing susceptibility to avian IAVs and the severity of seasonal IAVs. Recent research has underscored the role of innate immune system proteins (e.g., MxA and BTN3A3) in reducing human susceptibility to avian IAV H7N9 [4,5], while genetic variations in host genes, such as *IFITM3* and *IRF7,* predispose individuals to severe disease caused by H1N1pdm09 [6,7]. This emphasizes the critical role of host factors in impeding the spread of IAV strains and underscores the potential of the human immune system to defend against such infections.

The gut microbiota, a complex and highly diverse microbial community, serves as an essential mediator linking diseases to human genome evolution and is closely associated with the development and progression of many diseases [8,9]. Numerous studies have recognized the broad-reaching immune impact of the gut microbiota on pulmonary health [10–12]. A systematic review of gut microbiota changes in respiratory tract infection (RTI) patients consistently revealed decreased diversity, with depletion of *Firmicutes*, *Lachnospiraceae*, *Ruminococcaceae*, and *Ruminococcus*, and enrichment of *Enterococcus* [13]. Fecal transfer experiments have indicated that gut microbes from mice surviving H7N9 infection can confer resistance to naive recipient mice challenged with IAV [14]. Additionally, patients with IAV infection may experience symptoms resembling gastroenteritis [15], indicating the importance of the gut–lung axis in maintaining lung immunity homeostasis during influenza infection. Investigations have revealed significant changes in the composition of intestinal microbiota in individuals affected by different IAV subtypes, including H7N9 and H1N1 [16–18]. However, these studies have only established associations between gut microbiota and various IAV subtypes. Due to the potential confounding factors and reverse causality, the causal relationship between gut flora and IAV infection remains unclear.

Mendelian randomization (MR) provides an efficient approach to evaluating causal effects using genetic variants as instrumental variables (IVs) [19]. Genetic variants are randomly assigned during meiosis and not influenced by traditional confounding factors, such as environment, socioeconomic status, and behavior. Furthermore, genetic variants remain stable after birth, enabling the evaluation of chronologically plausible associations. Therefore, MR can overcome confounding and reverse causality issues inherent in traditional observational studies. MR analysis has been widely applied to assess causal effects between gut microbiota and diseases, such as autoimmune diseases and coronavirus disease 2019 (COVID-19) [20,21]. Xu et al. employed MR to investigate the causal effect of gut microbiota on seasonal influenza and influenza-induced pneumonia in Finland. In their study, the identification of intestinal flora was limited to the genus level [22]. In this study, we performed a systematic two-sample MR study to explore the causal effect of species-level gut microbiota on avian IAV H7N9 susceptibility and H1N1pdm09 severity in Chinese. Note that genome-wide association studies (GWAS) of H7N9 susceptibility have been restricted to Chinese populations thus far. The outcomes of this study might offer new insights for personalized IAV treatment through the regulation of gut microbiota.

2. Materials and Methods

2.1. Study Design

First, we conducted a two-sample MR analysis to investigate potential causal relationships between gut microbial features and IAV infection. Three different MR methods (refer to Methods further below) were performed to increase the robustness of the results and avoid bias. The selection of IVs adhered to three critical assumptions [19]: (i) Relevance: the IVs were associated with the exposure of interest; (ii) Independence: the IVs were independent of other confounding factors that affect both the exposure and outcome; (iii) Exclusion restriction: the IVs were required to influence the outcome solely through the

studied exposure. The stringent criteria for IV selection were essential to ensure the validity and robustness of the MR analysis results. Subsequently, protein–protein interaction (PPI) and functional enrichment analyses were carried out to investigate possible biological connections between gut microbiota and influenza infection. The study design is illustrated in Figure 1.

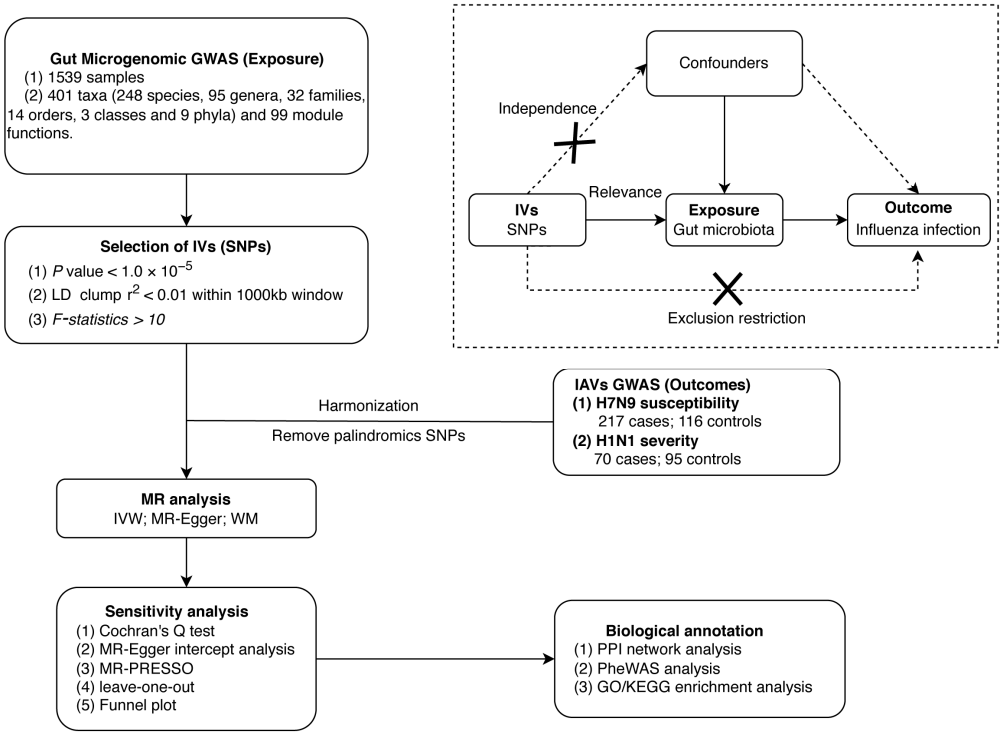

Figure 1. Overview of the process of Mendelian randomization analysis and major assumptions.

2.2. Gut Microbiome Data

The GWAS summary data for human gut microbiome composition were obtained from an extensive study [23], involving 1539 adult Chinese individuals with both blood and fecal samples available. Each participant underwent high-depth whole-genome and whole-metagenomic sequencing with a mean sequencing depth of 42× for the whole genome, ensuring precise genotyping. This dataset was composed of 500 microbial features, including 401 taxa (248 species, 95 genera, 32 families, 14 orders, 3 classes, and 9 phyla) and 99 module functions (MFs), all integrated into the analysis. The GWAS results for microbial features were meticulously adjusted for various factors, such as age, gender, body mass index, defecation frequency, stool form, 12 dietary and lifestyle factors, and the top four principal components (PCs), to minimize the effects of potential confounding factors [23].

2.3. H7N9 Susceptibility and H1N1 Severity GWAS Data

The summary statistics for H7N9 susceptibility were retrieved from a previous GWAS involving 217 H7N9 patients and 116 healthy poultry workers, all of Chinese descent [5]. Real-time reverse transcription polymerase chain reaction (RT–PCR) was used for diagnosing H7N9 infection, following the Diagnostic and Treatment Protocol for Human Infection with Avian Influenza A (H7N9) (http://www.nhc.gov.cn/gjhzs/s7952/201304/34750c7e6930463aac789b3e2156632f.shtml accessed on 30 May 2018). Similarly, summary statistics for H1N1 severity were collected from another preceding GWAS involving 165 Chinese H1N1pdm09 patients, confirmed by positive results of real-time RT–PCR [24]. Patients with mild symptoms (n = 95) were defined as outpatients not admitted to hospitals, while those with severe symptoms (n = 70) were hospitalized patients meeting specific criteria outlined in the Protocol for diagnosis and treatment of influenza (2019 version) [25]. All participants underwent high-depth whole-genome sequencing, with an average sequencing

depth exceeding 30×, to detect potential variants and for genotyping. Subsequently, GWAS summary statistics were generated using logistic regression analysis, adjusted for gender, age, and PCs.

2.4. Selection of IVs

The single nucleotide polymorphisms (SNPs) associated with microbiome features were chosen as eligible IVs according to several criteria. Firstly, SNPs with a p value $< 1 \times 10^{-5}$ were chosen to represent a broad range of microbiome [23,26]. To ensure independence, linkage disequilibrium (LD) clumping was performed ($r^2 < 0.01$ within a 1000 kb window) using the 1000 Genomes EAS population as a reference. SNPs with palindromic A/T or G/C alleles were excluded to prevent strand orientation or allele coding issues. SNPs associated with the outcome ($p < 1 \times 10^{-4}$) were also excluded. The strength of IVs was assessed using F-statistics, calculated using the formula [27]:

$$F = R^2(N - 1 - k)/(1 - R^2)k \quad (1)$$

where N represents the sample size, k indicates the number of IVs, and R^2 stands for the proportion of variance explained. For a SNP, R^2 was calculated using the equation:

$$R^2 = 2 \times EAF \times (1 - EAF) \times \beta^2 / [2 \times EAF \times (1 - EAF) \times \beta^2 + 2 \times EAF \times (1 - EAF) \times N \times SE^2] \quad (2)$$

where EAF is the effect allele frequency, β is the effect size, and SE is the standard error of effect size. SNPs with F-statistics < 10 were deemed insufficient in strength and were subsequently removed [28]. The independence of selected SNPs allowed for the calculation of the combined R^2 as the sum of individual R^2 values under the assumption of an additive model.

2.5. Two-Sample MR Analysis

The inverse variance weighted (IVW) test served as the primary method to evaluate causal effects, aggregating Wald ratios of IVs in a fixed-effect meta-analysis model, providing reliable results under the assumption of no horizontal pleiotropy for each IV [29]. Additionally, MR–Egger regression and the weighted median (WM) method were used for supplementary analysis. Suppose there are M genetic variants, where j represents the jth variant, with x denoting the exposure, and y signifying the outcome. The IVW method is a basic model assuming that pleiotropy does not exist or is zero. It estimated the causal effect (β_{xy}) by integrating the effect ratio ($\theta_j = \beta_{yj} / \beta_{xj}$) of genetic variant on outcome (β_{yj}) and exposure (β_{xj}) using inverse variance weighting. IVW estimates can also be obtained using the following weighted linear regression model without intercept terms:

$$\hat{\beta}_{yj} = b\hat{\beta}_{xj} + \varepsilon_j,\ \varepsilon_j \sim N\left(0,\ se\left(\beta_{yj}\right)^2\right) \quad (3)$$

The estimate of the slope parameter b is the causal effect, and the weight is the inverse of the variance of the genetic association effect corresponding to the outcome. In order to control the uncorrelated pleiotropy, MR–Egger identifies the violations of pleiotropy and heterogeneity by incorporating an intercept in the IVW model [30]. The regression model is as follows:

$$\hat{\beta}_{yj} = b_0 + b\hat{\beta}_{xj} + \varepsilon_j,\ \varepsilon_j \sim N\left(0,\ se\left(\beta_{yj}\right)^2\right) \quad (4)$$

Because some IVs may be pleiotropic, the WM method estimates the causal effect from the weighted median of the effect ratio (θ_j). The WM method offers consistent estimates even when up to 50% of the IVs are invalid [31]. Following the application of the Bonferroni correction, we established a statistically significant threshold of $p = 1 \times 10^{-4}$ (0.05/500). The associations with $p < 0.05$ but above 1×10^{-4} were considered nominally significant.

2.6. Sensitivity Analysis

Sensitivity analyses were conducted to assess the robustness of the MR analysis. MR–Egger intercept tests and MR–Pleiotropy Residual Sum and Outlier (MR–PRESSO) global tests were used to examine horizontal pleiotropy [32,33]. Additionally, Cochran's Q statistic and a funnel plot were used to examine heterogeneity [34]. A leave-one-out analysis was conducted to demonstrate that inferred causal relationships were not influenced by a single SNP [32]. All MR analyses were carried out using R software (version 4.1.2) and the "TwoSampleMR" package (version 0.5.6).

2.7. Biological Annotation

ANNOVAR (version 20180416) was used to functionally annotate variants with $p < 1 \times 10^{-4}$ in H7N9 susceptibility and H1N1 severity GWAS, and variants with $p < 1 \times 10^{-5}$ in the gut microbiome GWAS [35]. PPI networks were constructed using shared positional mapped genes between IAVs and the gut microbiome. These networks were predicted using the Search Tool for the Retrieval of Interacting Genes (STRING, version 12.0) online database [36]. A combined score ≥ 0.4 was chosen for construction of the PPI networks. We also extracted the functional enrichment results for human phenotype (Experimental Factor Ontology [37] and Human Phenotype Ontology [38]) from STRING, which could provide insight into the associations of genes with various phenotypes. The connected PPI networks were visualized using Cytoscape software (version 3.8.0) [39]. The top 10 nodes were identified as hub genes using the Maximal Clique Centrality (MCC) method with the CytoHubba plug-in (version 0.1) [40]. The effect of hub genes on multiple phenotypes was evaluated through Phenome-Wide Association Study (PheWAS) by examining the pleiotropy of hub genes in the summary statistics for 4756 complex traits and diseases across 28 domains using the GWAS ATLAS [41]. PheWAS offered a more comprehensive understanding of the biological significance of these genes and helped elucidate the MR results. The statistically significant threshold was defined as 1.05×10^{-5} (0.05/4756). IVs for pairs of microbial features and IAVs with significant causality were annotated using ANNOVAR. Additionally, Gene Ontology (GO) [42,43] and Kyoto Encyclopedia of Genes and Genomes (KEGG) [44] pathway enrichment analyses were performed for the positional mapped genes using DAVID (https://david.ncifcrf.gov/tools.jsp accessed on 21 January 2024) [45,46] to reveal the potential underlying biological pathways or functions of causal associations. GO is utilized as a bioinformatics tool for annotating genes and analyzing the biological processes they are involved in. It classifies gene functions into biological processes (BP), molecular functions (MF), and cellular components (CC). KEGG is a database for analyzing molecular signaling pathways and interactions in biological systems. A significance threshold of $p < 0.05$ and Fold Enrichment > 2.5 was considered statistically significant. The enrichment analysis results are visualized by SRplot web server (http://www.bioinformatics.com.cn/SRplot accessed on 21 January 2024) [47].

3. Results

3.1. Effect of Gut Microbiota on H7N9 Susceptibility

The results of the MR analysis concerning H7N9 susceptibility are detailed in Figure S1. The genetic IVs varied from 2 to 29 across different gut microbiome features. *F*-statistics for the human gut microbiota ranged from 20.17 to 37.02, all surpassing 10, indicating a reduced susceptibility to weak instrument bias. Initially, the IVW method identified 14 gut bacterial taxa associated with H7N9 susceptibility (Figure 2, Table S1). The effect directions estimated by MW were consistent with those derived from IVW. However, the MR–Egger method revealed inconsistent directions for two gut bacterial taxa, including the genus *Rahnella* and *Coprococcus catus*. Subsequently, 12 gut bacterial taxa were found to be nominally causally associated with H7N9 susceptibility with statistical significance. It is worth noting that *Clostridium hylemonae* ($\beta = -0.335$, 95% CI: -0.622 to -0.049, $p = 0.022$) and *Clostridium ramosum* ($\beta = -0.390$, 95% CI: -0.684 to -0.096, $p = 0.009$), known for synthesizing short-chain fatty acids (SCFAs), exhibited a negative correlation with the

susceptibility to H7N9. Additionally, *Streptococcus peroris* (β = −0.327, 95% CI: −0.648 to −0.006, p = 0.046) and *Streptococcus sanguinis* (β = −0.552, 95% CI: −1.017 to −0.087, p = 0.020)) were associated with a reduced risk of H7N9 susceptibility, while *Streptococcus mitis* (β = 0.504, 95% CI: 0.022 to 0.986, p = 0.041) showed an increased risk of H7N9 susceptibility. Scatter plots are displayed in Figure S2.

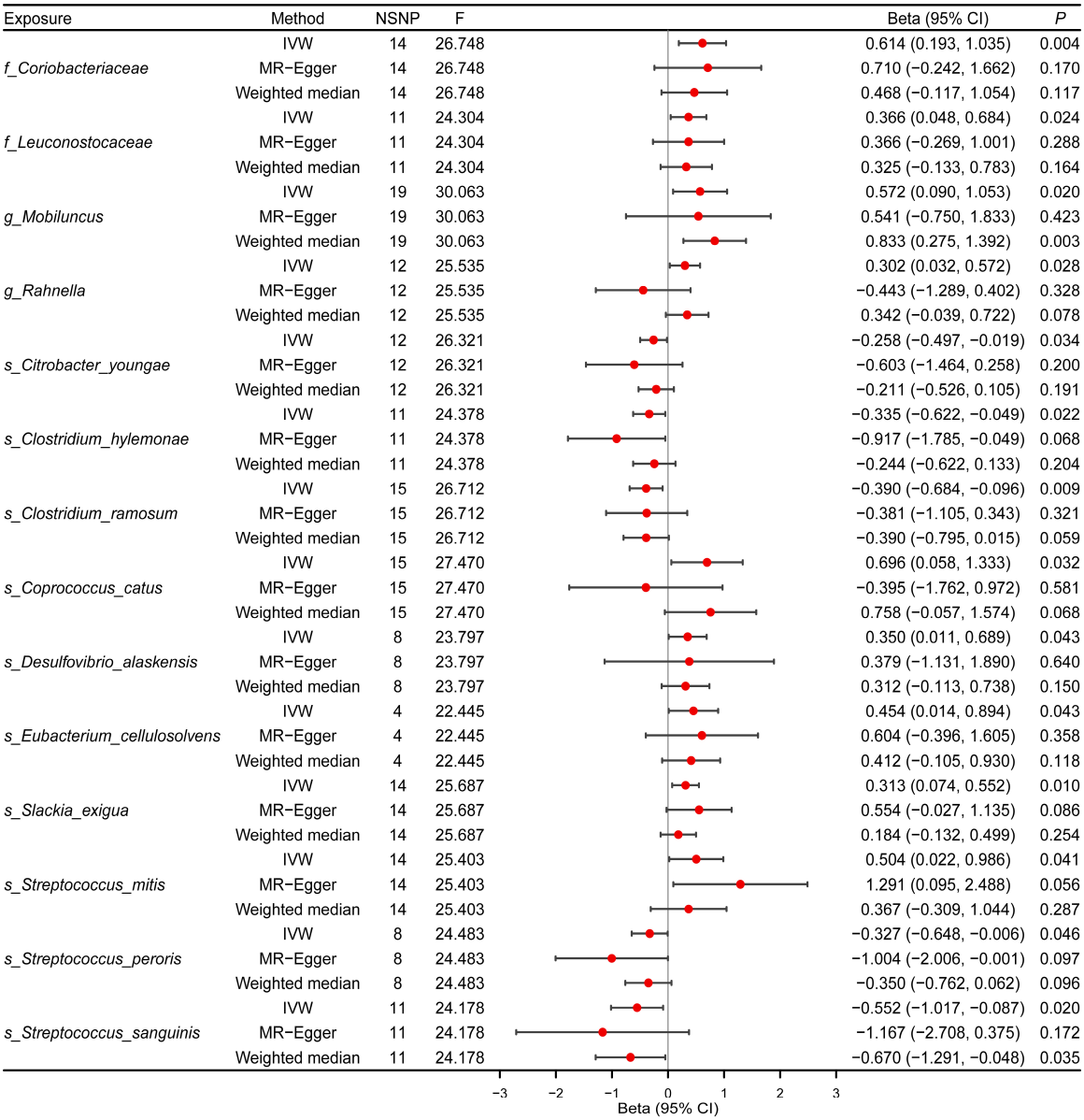

Figure 2. Causal effects of gut microbiota on H7N9 susceptibility. Summary of Mendelian randomization (MR) estimates derived from inverse variance weighted (IVW), weighted median (WM), and MR–Egger analyses. CI denotes confidence interval; OR, odds ratio; SNPs, single nucleotide polymorphisms. "s_", "g_", "f_" are species, genus, and family, respectively.

In the sensitivity analysis (Table 1), both the MR–PRESSO Global test and MR–Egger intercept test indicated a limited impact of horizontal pleiotropy. Furthermore, Cochran's Q test suggested no significant heterogeneity. The leave-one-out analysis indicated that no SNPs significantly influenced the overall result (Figure S3). Most funnel plots demonstrated symmetry (Figure S4), reinforcing the robustness and reliability of the MR analysis results.

Table 1. Sensitivity analysis of the causal effect between gut microbiota and H7N9 susceptibility.

Exposure	Method	Heterogeneity Q	Heterogeneity Q_df	Heterogeneity Q_pval	Pleiotropy Egger Intercept Pval	MR–PRESSO Global Test Pval
f_Coriobacteriaceae	MR–Egger	9.371	12	0.671	0.830	0.754
	IVW	9.419	13	0.741		
f_Leuconostocaceae	MR–Egger	8.736	9	0.462	1.000	0.592
	IVW	8.736	10	0.557		
g_Mobiluncus	MR–Egger	28.293	17	0.042	0.961	0.083
	IVW	28.298	18	0.058		
g_Rahnella	MR–Egger	6.428	10	0.778	0.098	0.600
	IVW	9.751	11	0.553		
s_Citrobacter youngae	MR–Egger	6.861	10	0.738	0.433	0.766
	IVW	7.529	11	0.755		
s_Clostridium hylemonae	MR–Egger	3.534	9	0.939	0.198	0.858
	IVW	5.469	10	0.858		
s_Clostridium ramosum	MR–Egger	6.906	13	0.907	0.978	0.930
	IVW	6.907	14	0.938		
s_Coprococcus catus	MR–Egger	13.319	13	0.424	0.106	0.347
	IVW	16.410	14	0.289		
s_Desulfovibrio alaskensis	MR–Egger	3.362	6	0.762	0.970	0.878
	IVW	3.364	7	0.849		
s_Eubacterium cellulosolvens	MR–Egger	0.018	2	0.991	0.773	0.983
	IVW	0.127	3	0.988		
s_Slackia exigua	MR–Egger	5.910	12	0.921	0.390	0.913
	IVW	6.706	13	0.917		
s_Streptococcus mitis	MR–Egger	7.813	12	0.800	0.184	0.701
	IVW	9.798	13	0.710		
s_Streptococcus peroris	MR–Egger	5.576	6	0.472	0.213	0.430
	IVW	7.515	7	0.377		
s_Streptococcus sanguinis	MR–Egger	4.667	9	0.862	0.433	0.862
	IVW	5.339	10	0.867		

Abbreviations: IVW, inverse variance weighted; MR–PRESSO, MR–pleiotropy residual sum and outlier. "s_", "g_", "f_" are species, genus, family, order, class, and phylum, respectively.

3.2. Effect of Gut Microbiota on H1N1 Severity

Causal effects of all gut microbiota on H1N1 severity are presented in Figure S5. The genetic IVs for each gut microbiome feature ranged from 7 to 31, with *F*-statistics ranging from 23.38 to 30.70, surpassing the empirical threshold of 10. The IVW analysis identified 18 gut bacterial taxa associated with H1N1 severity. However, alternative MR analysis methods revealed inconsistent effect directions for three bacterial species: *Roseburia intestinalis*, *Treponema vincentii*, and *Veillonella atypica*. Ultimately, 15 gut bacterial taxa met the criteria as significant contributors to the development of H1N1 severity (Figure 3, Table S2). In particular, *Faecalibacterium prausnitzii* ($\beta = -0.394$, 95% CI: -0.774 to -0.013, $p = 0.043$), playing a key role in the biosynthesis of SCFAs, exhibited a negative association with the risk of H1N1 severity. Moreover, *Streptococcus parasanguinis* ($\beta = -0.574$, 95% CI: -1.004 to -0.144, $p = 0.009$) and *Streptococcus suis* ($\beta = -0.455$, 95% CI: -0.865 to -0.044, $p = 0.030$) were also correlated with a reduced risk of H1N1 severity. Scatter plots are available in Figure S6.

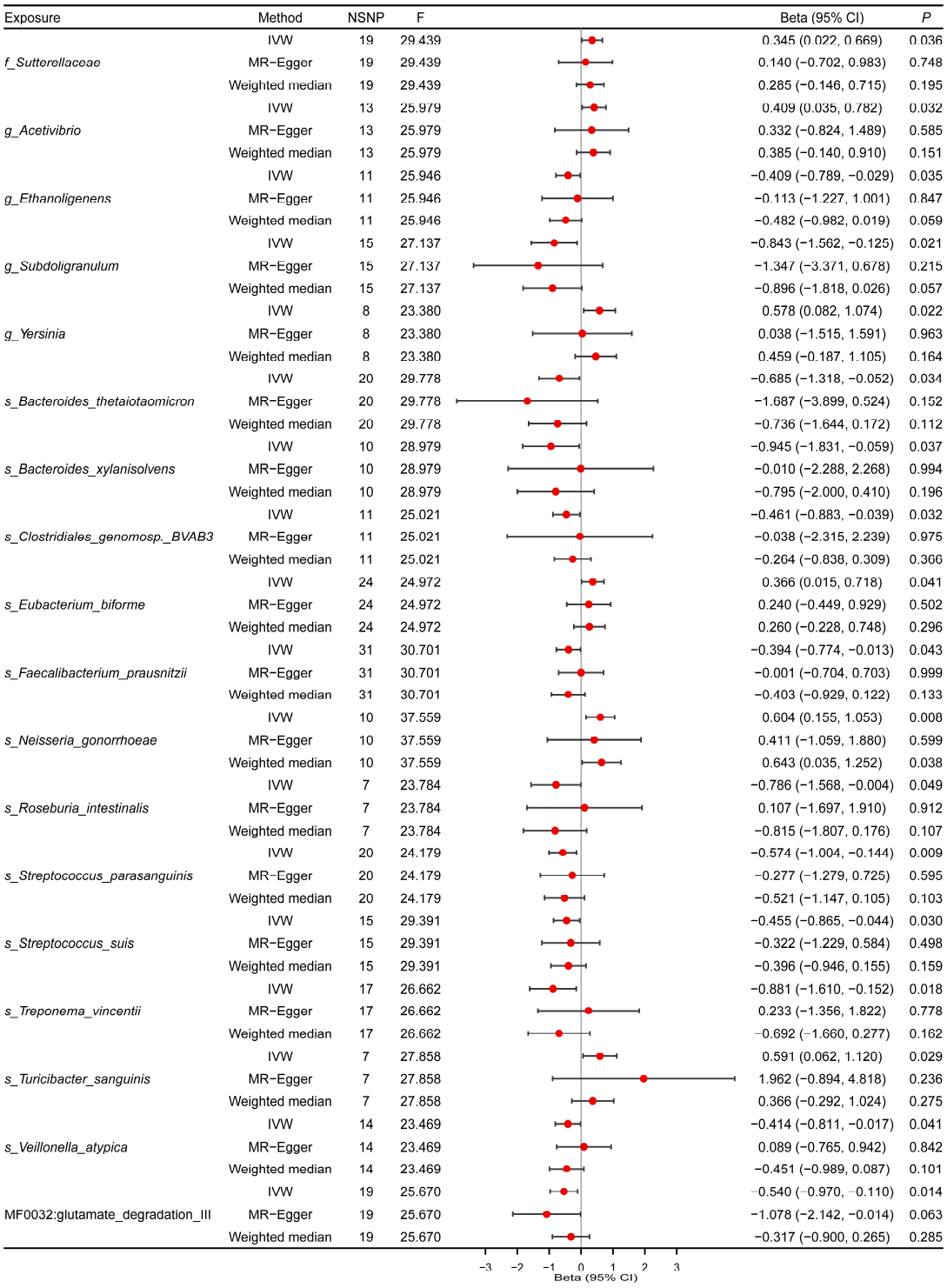

Figure 3. Causal effects of gut microbiota on H1N1 severity. Summary of Mendelian randomization (MR) estimates obtained from inverse variance weighted (IVW), weighted median (WM), and MR–Egger analyses. CI, confidence interval; SNPs, single nucleotide polymorphisms. "s_", "g_", "f_" are species, genus, and family, respectively.

Based on the results of sensitivity analysis, no significant horizontal pleiotropy or heterogeneity was detected using the MR–Egger intercept test, MR–PRESSO global test and Cochran's Q test (Table 2). Furthermore, the leave-one-out analysis and funnel plots demonstrated the stability of the findings (Figures S7 and S8).

Table 2. Sensitivity analysis of the causal effect between gut microbiota and H1N1 severity.

Exposure	Method	Heterogeneity Q	Heterogeneity Q_df	Heterogeneity Q_pval	Pleiotropy Egger Intercept Pval	MR–PRESSO Global Test Pval
f_Sutterellaceae	MR–Egger	10.309	17	0.890	0.612	0.911
	IVW	10.576	18	0.911		
g_Acetivibrio	MR–Egger	8.999	11	0.622	0.894	0.725
	IVW	9.018	12	0.701		
g_Ethanoligenens	MR–Egger	4.722	9	0.858	0.593	0.894
	IVW	5.029	10	0.889		
g_Subdoligranulum	MR–Egger	4.104	13	0.990	0.611	0.992
	IVW	4.375	14	0.993		
g_Yersinia	MR–Egger	2.935	6	0.817	0.499	0.850
	IVW	3.453	7	0.840		
s_Bacteroides_thetaiotaomicron	MR–Egger	15.037	18	0.659	0.366	0.673
	IVW	15.897	19	0.664		
s_Bacteroides_xylanisolvens	MR–Egger	6.308	8	0.613	0.408	0.645
	IVW	7.071	9	0.630		
s_Clostridiales_genomosp._BVAB3	MR–Egger	9.242	9	0.415	0.719	0.535
	IVW	9.384	10	0.496		
s_Eubacterium_biforme	MR–Egger	17.371	22	0.743	0.680	0.790
	IVW	17.546	23	0.782		
s_Faecalibacterium_prausnitzii	MR–Egger	24.531	29	0.702	0.203	0.706
	IVW	26.226	30	0.664		
s_Neisseria_gonorrhoeae	MR–Egger	5.220	8	0.734	0.793	0.821
	IVW	5.294	9	0.808		
s_Roseburia_intestinalis	MR–Egger	1.476	5	0.916	0.331	0.873
	IVW	2.636	6	0.853		
s_Streptococcus_parasanguinis	MR–Egger	12.312	18	0.831	0.528	0.862
	IVW	12.726	19	0.852		
s_Streptococcus_suis	MR–Egger	7.267	13	0.888	0.754	0.914
	IVW	7.369	14	0.920		
s_Treponema_vince	MR–Egger	14.963	15	0.454	0.147	0.413
	IVW	17.306	16	0.366		
s_Turicibacter_sanguinis	MR–Egger	3.302	5	0.653	0.382	0.671
	IVW	4.219	6	0.647		
s_Veillonella_atypica	MR–Egger	9.639	12	0.648	0.217	0.584
	IVW	11.338	13	0.583		
MF0032:glutamate_degradation_III	MR–Egger	8.588	17	0.952	0.294	0.948
	IVW	9.761	18	0.939		

Abbreviations: IVW, inverse variance weighted; MR–PRESSO, MR–pleiotropy residual sum and outlier. "s_", "g_", "f_" are species, genus, family, order, class, and phylum, respectively.

3.3. Biological Annotation

We identified a total of 87 shared GWAS significant genes connecting H7N9 susceptibility and microbiota features (Table S3) and 30 shared genes of H1N1 severity and microbiota features (Table S4). The PPI network analysis of both gene sets using the STRING database revealed a significantly higher number of interactions than expected by chance. By evaluating the enrichment of observed edges compared to expected edges, we obtained a PPI p-value of 8.43×10^{-8} for 87 proteins (Figure S9A) and 3.70×10^{-3} for 30 proteins (Figure S9B), indicating a biological connection to some extent. According to STRING, previous studies found that these genes were associated with several phenotypes at a false

discovery rate (FDR) < 0.05. For the overlapping proteins between H7N9 susceptibility and microbiota features, we identified a significant enrichment of 44 phenotypes (Table S5), including gut microbiome measurement, susceptibility to infectious disease measurement, respiratory disease biomarker, etc. In contrast, we observed a significant enrichment of only three phenotypes among the overlapping proteins between H1N1 severity and microbiota features (Table S6).

The connected PPI networks were visualized using Cytoscape (Figure 4), and hub genes were screened (Tables S7 and S8). Except for *ZBTB18* and *C1orf100*, all hub genes were associated with multiple phenotypes ($p < 1.05 \times 10^{-5}$). In the PPI network linking H7N9 susceptibility to microbiota features, PheWAS results revealed that 8 out of 10 hub genes (*LRP1B*, *ROBO2*, *USH2A*, *FOXP1*, *TENM4*, *CACNA1C*, *PCLO*, and *AGRN*) showed enrichment with genetic signals associated with the metabolic or nutritional domain. Moreover, 4 of the 10 hub genes (*LRP1B*, *FOXP1*, *CACNA1C*, and *KALRN*) were enriched with genetic signals associated with the immunological domain (Figure S10, Table S9). Similarly, 8 of 10 hub genes (*PTPRD*, *RARB*, *PPARGC1A*, *SORCS2*, *MED15*, *DLGAP1*, *PLCB4*, and *DGKB*) in the network connecting H1N1 severity to microbiota features showed enrichment with the metabolic or nutritional domain. However, only one hub gene (*PPARGC1A*) was enriched with the immunological domain (Figure S11, Table S10). In summary, PPI networks and PheWAS analysis uncover the connection between IAV infection and microbial features, which are associated with hub genes, as well as the metabolic or nutritional domain and the immunological domain.

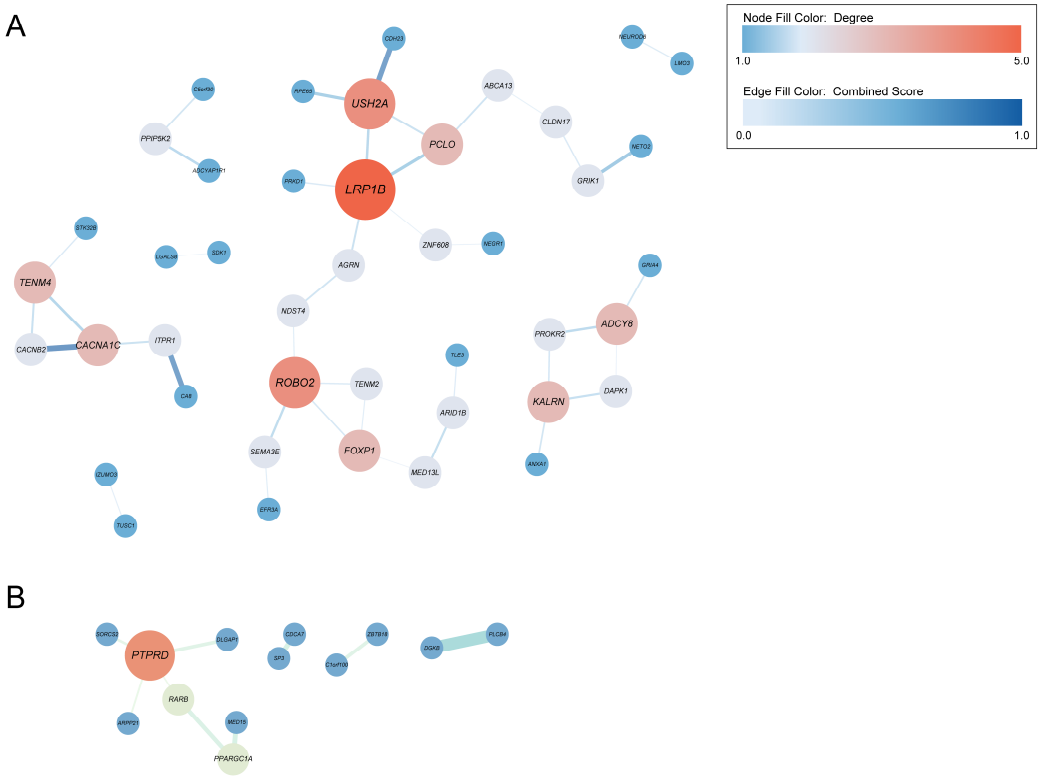

Figure 4. Visualization of connected protein-protein interaction networks using Cytoscape. (**A**) The network of overlapped genes between H7N9 susceptibility and microbiota features. (**B**) The network of overlapped genes between H1N1 severity and microbiota features. Node size and color correspond to the respective degrees, while edge weight and color are proportional to the STRING confidence score.

A total of 170 IVs for the 12 pairs of microbial features and H7N9 susceptibility with potential causality were mapped onto 216 genes (Table S11), and 232 IVs for the 15 pairs of microbial features and H1N1 severity were mapped onto 304 genes (Table S12). The GO

analysis showed that both gene sets were significantly enriched in several terms, including cell–cell junction assembly, adherens junction organization, cell–cell adhesion mediated by cadherin, cell–cell adhesion via plasma-membrane adhesion molecules, calcium-dependent cell–cell adhesion via plasma membrane cell adhesion molecules, and homophilic cell adhesion via plasma membrane adhesion molecules. Additionally, the 216 mapped genes were significantly enriched in galactosylceramide catabolic process, phosphorylation, while the 304 mapped genes were significantly enriched in transmembrane receptor protein tyrosine kinase signaling pathway, Ras protein signal transduction, positive regulation of T-helper cell differentiation, etc. (Figure 5, Tables S13 and S14). In the KEGG analysis, the 216 mapped genes did not show significantly enriched pathways, whereas the 317 mapped genes were significantly enriched in the Rap1, Apelin, and calcium signaling pathways (Figure S12, Table S15).

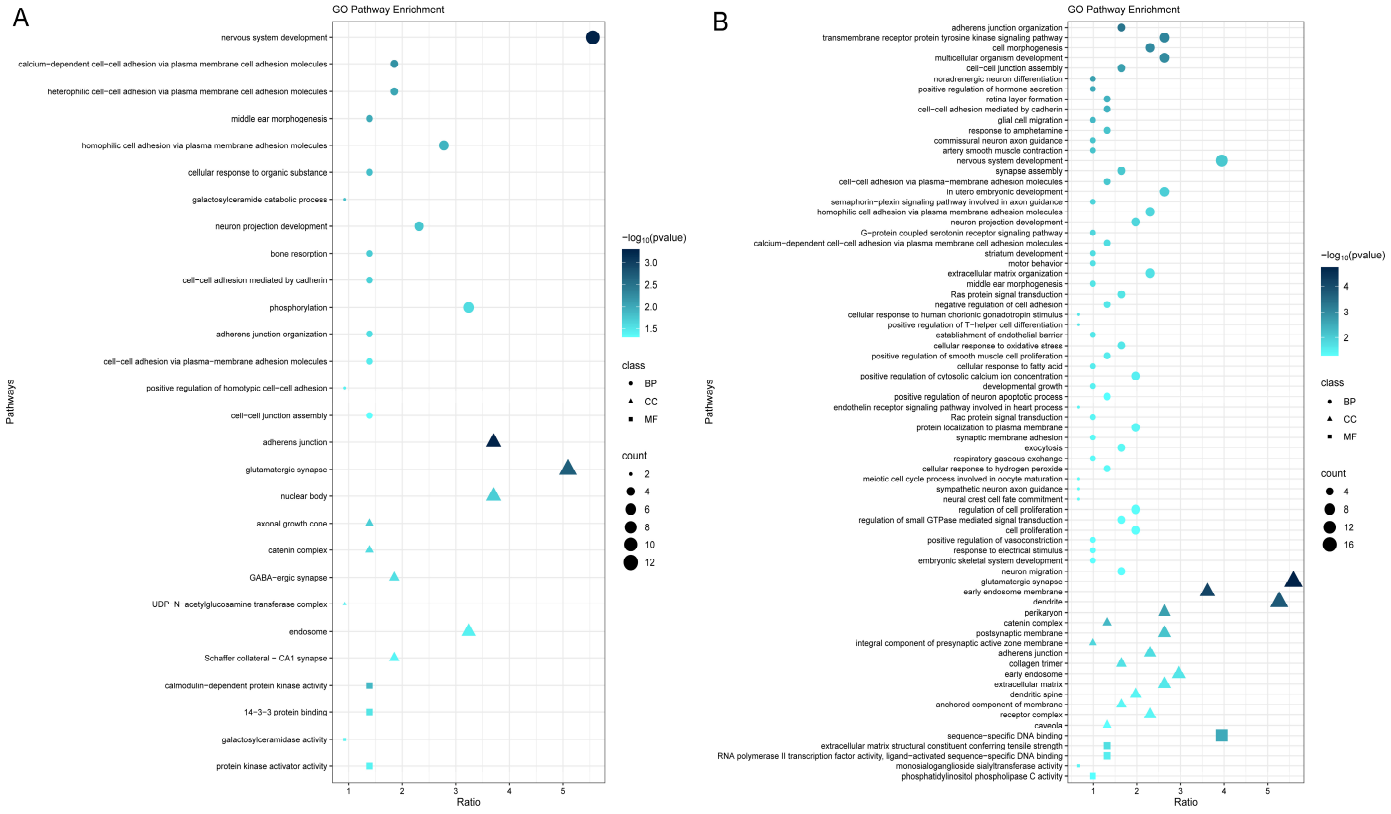

Figure 5. Gene Ontology pathway enrichment analysis performed on (**A**) 216 genes annotated from instrumental variables for pairs of microbial features and H7N9 susceptibility with potential causal relationships in Mendelian randomization (MR), and (**B**) 314 genes annotated from IVs for pairs of microbial features and H1N1 severity with potential causal relationships in MR. BP: biological process, CC: cellular component, MF: molecular function.

4. Discussion

Our research revealed that 12 specific bacterial features were causally associated with H7N9 susceptibility, while 15 bacterial features were causally associated with the severity of H1N1, underscoring the significance of the gut–lung axis in regulating immune responses during IAV infections. We also provided a possible biological interpretation of the association between gut microbiota and IAV infection using gene- and gene-set-based analyses on multi-omics data.

The complex and diverse microbial ecosystem in the gastrointestinal tract plays a pivotal role in maintaining human health. Recent studies have demonstrated the intricate interplay between gut microbiota and immune system regulation, extending its impact beyond the gut to encompass the entire body, including distant organs such as

the lungs [48–50]. The gut–lung axis, representing the interaction between gastrointestinal bacteria and the pulmonary system, can modulate inflammatory activity at both local and systemic levels [51]. Notably, in the treatment of IAV-induced viral respiratory infections, the significant disruption of the gut microbial ecosystem by antibiotics can compromise the innate and adaptive defenses of the host, emphasizing the essential role of the gut–lung axis in IAV infection [52,53]. Furthermore, emerging evidence has underscored the critical role of microbiota composition in regulating the development of virus-specific CD4 and CD8 T cells, as well as antibody responses, in respiratory influenza virus infections [53]. Disruptions in gut microbes could potentially impair immune cell migration to the lungs, thereby increasing susceptibility to respiratory tract infections [54,55]. This observation emphasized the pivotal role of gut microbiota in shaping host immune responses and underscored the potential for modulating microbiota composition as a new therapeutic approach for treating influenza and other respiratory viral infections.

There is mounting evidence linking the composition of gut microbiota to IAV infections, with the fecal microbiomes of H1N1 and H7N9 patients showing a noticeable decrease in bacterial diversity [16,17]. It is worth noting that gut dysbiosis, often characterized by reduced microbial diversity, is commonly associated with inflammatory and autoimmune disorders [51]. In patients with laboratory-confirmed H1N1, a reduction in the phyla *Actinobacteria* and *Firmicutes*, along with the genera *Faecalibacterium* and *Streptococcus*, was observed compared to healthy controls [16]. Similarly, in a study involving 26 patients infected with H7N9, a decrease in the phyla of *Bacteroidetes* and the genera of *Eubacterium*, *Roseburia*, and *Faecalibacterium*, as well as the species of *Roseburia intestinalis* and *Faecalibacterium prausnitzii*, was noted, while an enrichment was observed for the genus of *Veillonella* [17].

Consistent with previous research, our study identified that six out of eight bacterial taxa negatively associated with H1N1 severity belonged to the phylum *Firmicutes*, with the exception of *Bacteroides thetaiotaomicron* and *Bacteroides xylanisolvens*. Similarly, apart from *Citrobacter youngae*, the other four bacterial taxa negatively linked to H7N9 susceptibility also belonged to *Firmicutes*. Previous studies have reported a reduction in *Firmicutes* among patients with RTIs, including H1N1 infection, COVID-19, tuberculosis (TB), community-acquired pneumonia, and recurrent respiratory tract infections [13]. Certain gut microbes, notably *Faecalibacterium prausnitzii* and *Clostridium hylemonae* of the *Firmicutes* phylum, possess a strong ability to produce SCFAs, such as acetate, propionate, and butyrate, through the fermentation of dietary fiber and resistant starch [56,57]. Microbiota-derived butyrate activates the nuclear receptor peroxisome proliferator activated receptor γ in colonic epithelial cells, shifting their energy metabolism towards fatty acid oxidation and oxidative phosphorylation in mitochondria, which consumes high levels of oxygen [58–60]. This suggests that SCFAs promote gut homeostasis through a positive feedback loop by limiting the luminal bioavailability of oxygen. SCFAs can also signal through the membrane receptor G protein-coupled receptor (GPR) to activate signaling pathways that regulate immune functions [61]. Research has shown that acetate could protect against respiratory syncytial virus-induced disease by activating GPR43 and modulating type 1 responses in lung epithelial cells [62]. Moreover, SCFAs can induce both effector and regulatory T cells to regulate the immune system by inhibiting the direct histone deacetylase (HDAC) in T cells and enhancing the mTOR-S6K pathway [63]. In our study, *Faecalibacterium prausnitzii*, a representative bacterium of the phylum *Firmicutes*, was also found to be negatively correlated with H1N1 severity. *Faecalibacterium prausnitzii* is considered as an anti-inflammatory probiotic that provides defense against various gastrointestinal disorders [64]. Reduced levels of *Faecalibacterium prausnitzii* have been observed in patients with COVID-19, TB, asthma, and cystic fibrosis [65–68]. Additionally, a study investigating the correlations between gut microbiota and persistent symptoms in recovered COVID-19 patients revealed a negative correlation between chest tightness after activity and the relative abundance of *Faecalibacterium prausnitzii* [69].

Our results indicated that the species *Streptococcus peroris* and *Streptococcus sanguinis*, as well as *Streptococcus parasanguinis* and *Streptococcus suis*, were negatively correlated with H7N9 susceptibility and H1N1 severity, respectively. However, concerning the genus *Streptococcus*, different outcomes were observed in individuals infected with H1N1 and H7N9 compared to the control group, showing decreased levels for H1N1 and elevated levels for H7N9 [16,17]. Animal studies have indicated that pre-exposure to *Streptococcus suis* improved survival in mice co-infected with the influenza virus, with the upregulated innate immunity potentially playing a significant role in reducing mortality when the bacteria were administered before viral infection [70]. Furthermore, a clinical trial demonstrated that the estimated risk of respiratory failure during the course of COVID-19 was significantly lower by eightfold in the group receiving oral bacteriotherapy with streptococcal-containing preparations compared to the untreated group. Conversely, the incidence of ICU admission and mortality was higher among patients not treated with oral bacteriotherapy [71]. The bacterial strains present in the bacterial formulation enhanced the production of both nuclear factor erythroid 2p45-related factor 2 and its target Heme oxygenase-1, exerting antiviral effects through the reduction of oxidative stress [72]. Interestingly, Xu et al. reported that the genus *Streptococcus* was negatively associated with influenza outcomes in FinnGen cohorts, consistent with our findings in the Chinese population [22]. However, we also found that *Streptococcus mitis* was positively associated with H7N9 susceptibility. *Streptococcus mitis* is a predominant cause of infective endocarditis and bacteremia. It is notable that the majority of virulence factors identified in the *Streptococcus pneumoniae* genome are shared with *Streptococcus mitis* [73]. These findings suggest that not all *Streptococcus* species provide protection against influenza. In particular, *Streptococcus mitis* appears to be a potential risk factor for susceptibility to H7N9.

In our study, we identified hub genes such as *LRP1B* and *PTPRD* that serve as key connections between IAV infection and microbiota features. *LRP1B*, which belongs to the low-density lipoprotein (LDL) receptor family, plays diverse roles in normal cell function and development by interacting with multiple ligands. The LDL receptor family has roles related to the clearance of extracellular ligands and is proposed to be involved in extracellular signal transduction [74]. A previous GWAS study demonstrated an association between *LRP1B* and Influenza A (H1N1) infection [75]. Depletion of *LRP1B* has been shown to reduce IAV A/Puerto Rico/8/34 H1N1 infection [76] and influenza A/WSN/33 replication [77]. *PTPRD* encoded a member of the protein tyrosine phosphatase (PTP) family. PTPs are known to be signaling molecules that regulate a variety of cellular processes, including cell growth, differentiation, mitotic cycle, and oncogenic transformation [78]. *PTPRD* is involved in various signaling pathways, including PTPRD/STAT3/JAK and PTPRD/PD-1/PD-L1 axes [79–82]. These pathways are crucial in regulating IAV replication and anti-IAV immunity [83,84]. Moreover, PheWAS analysis revealed connections between hub genes and metabolic, nutritional, and immunological traits. GO enrichment highlighted a significant association between genes derived from IAVs and the BP of adherens junctions. Adherens junctions are formed by the transmembrane adhesion molecule vascular endothelial (VE)-cadherin and its cytoplasmic tail binding molecules, like β-catenin and plakoglobin, which anchor to actin via α-catenin and stabilize the junction [85]. The Rap1 signaling pathway, identified through KEGG enrichment, plays a critical role in regulating cell adhesion and cell–cell junction formation by modulating the function of integrins and other adhesion molecules in various cell types. Notably, gut microbiota could influence endothelial cell function at distant sites, such as the liver [86]. During IAV infection, the virus affects VE cells by inducing β-catenin degradation in adherens junctions, which is one of the key mechanisms leading to vascular hyperpermeability in severe influenza [87]. Therefore, a plausible mechanism for the causal relationship between gut microbiota and IAV infection may involve the regulation of adherens junctions in endothelial cells during the course of IAV infection.

This study had several strengths. Firstly, we utilized the largest-scale metagenomics GWAS dataset available for individuals of Chinese ancestry. Despite the relatively small

sample size of the H1N1 and H7N9 GWAS, they represented the most extensive GWAS study on avian IAV susceptibility conducted to date. Secondly, the application of metagenomic sequencing techniques allowed for precise bacterial classification down to the species level. Through the analysis of biologically relevant samples, metagenomes provided a comprehensive view of the gut microbial community, offering unparalleled insights into bacterial diversity and composition. Thirdly, our study adopted a two-sample MR approach to estimate causal effects and integrated three sensitivity analysis techniques to ensure robustness and mitigate potential pleiotropy from the IVs. By employing a rigorous analytical framework, the study aimed to provide accurate quantitative estimates of the causal relationship, thereby enhancing confidence in the validity of the findings. Our results revealed the correlations between gut microbiota composition and avian IAV infection, suggesting the potential utility of gut microbiota as a targeted risk assessment tool for the disease and as a potential therapeutic strategy.

There were several limitations in this study. Firstly, the ethnic homogeneity of the research population necessitates caution when extrapolating our findings to individuals of different races. Secondly, although we adopted one of the largest gut metagenomics and IAV GWAS datasets to date, the sample size remained modest, and the number of loci examined was relatively limited. Therefore, further research based on larger GWAS datasets is crucial to validate our observations and establish the generalizability of the findings across diverse populations. Thirdly, our findings were not corroborated by in vivo flora colonization assay.

Despite these limitations, we believe that our findings provided new clues for further investigation of microbial function via microbiota colonization in vivo. Focusing on gut microbiota could represent an innovative approach to the prophylaxis and therapy of IAV infections.

5. Conclusions

Our MR study has successfully identified the potential causal effects of 12 and 15 gut microbial features on H7N9 infection and H1N1pdm09 severity, respectively. In particular, *Clostridium hylemonae* and *Faecalibacterium prausnitzii*, which promote the production of SCFAs, were negatively associated with H7N9 susceptibility and H1N1pdm09 severity separately. These findings not only highlight the significant implications for understanding the pathogenesis of IAV infection but also provide valuable clues for future research to elucidate the role of gut microbiota in infectious diseases.

In summary, our study not only expands our knowledge concerning the impact of the gut microbiota on H7N9 susceptibility and H1N1pdm09 severity but also underscores the potential for targeting gut microbial composition based on these findings. The causally related bacterial groups open a promising avenue for the development of novel preventative and therapeutic strategies against IAV and other respiratory tract infections. An in-depth comprehension of the foundational mechanisms will facilitate the development of efficacious strategies to modulate the gut microbiome, thereby reducing the incidence and severity of IAV infections.

Supplementary Materials: The following supporting information can be downloaded at: https://www.mdpi.com/article/10.3390/microorganisms12061170/s1, Figure S1: The circus plot showing the MR results of all gut microbiota on H7N9 susceptibility. Circles from outside are the *p*-value of IVW, the beta for IVW, the beta for MR–Egger, the beta for WM and the F-statistics. The outermost circle is the ID of each gut microbiota. "s_", "g_", "f_", "o_", "c_", "p_" are species, genus, and family, order, class, phyla respectively. IVW, inverse variance weighted; WM, weighted median; Figure S2: Scatter plots for the significant MR associations ($p < 0.05$) between gut microbiota and H7N9 susceptibility. "s_", "g_", "f_" are species, genus, and family, respectively; Figure S3: Forest plots for the leave-one-out analysis of the significant MR associations ($p < 0.05$) between gut microbiota and H7N9 susceptibility. "s_", "g_", "f_" are species, genus, and family, respectively; Figure S4: Funnel plots for the significant MR associations ($p < 0.05$) between gut microbiota and H7N9 susceptibility. "s_", "g_", "f_" are species, genus, and family, respectively; Figure S5: The circus plot showing the MR

results of all gut microbiota on H1N1 severity. Circles from outside are the *p*-value of IVW, the beta for IVW, the beta for MR–Egger, the beta for WM and the F-statistics. The outermost circle is the ID of each gut microbiota. "s_", "g_", "f_", "o_", "c_", "p_" are species, genus, and family, order, class, phyla respectively. IVW, inverse variance weighted; WM, weighted median; Figure S6: Scatter plots for the significant MR associations ($p < 0.05$) between gut microbiota and H1N1 severity. "s_", "g_", "f_" are species, genus, and family, respectively; Figure S7: Forest plots for the leave-one-out analysis of the significant MR associations ($p < 0.05$) between gut microbiota and H1N1 severity. "s_", "g_", "f_" are species, genus, and family, respectively; Figure S8: Funnel plots for the significant MR associations ($p < 0.05$) between gut microbiota and H1N1 severity. "s_", "g_", "f_" are species, genus, and family, respectively; Figure S9: Comprehensive overview of PPI networks, including (A) 87 shared genes and (B) 30 shared genes predicted by STRING. Line color indicates the type of interaction evidence; Figure S10: PheWAS plots for hub genes in the PPI network of overlapped genes between H7N9 susceptibility and microbiota features. Bonferroni corrected $p = 1.05 \times 10^{-5}$; Figure S11: PheWAS plots for hub genes in the PPI network of overlapped genes between H1N1 severity and microbiota features. Bonferroni corrected $p = 1.05 \times 10^{-5}$; Figure S12: KEGG pathway enrichment analysis performed on 314 genes annotated from IVs for pairs of microbial features and H1N1 severity with potential causal relationships in two-sample Mendelian randomization; Table S1: Summary of causal association between gut microbial features and H7N9 susceptibility; Table S2: Summary of causal association between gut microbial features and H1N1 severity; Table S3: Shared positional mapped genes of H7N9 susceptibility and microbiota features; Table S4: Shared positional mapped genes of H1N1 severity and microbiota features; Table S5: Human phenotype enrichment analysis of 87 proteins connecting H7N9 susceptibility and microbiota features; Table S6: Human phenotype enrichment analysis of 30 proteins connecting H1N1 severity and microbiota features; Table S7: The hub genes ranked by MCC method in PPI network of overlapped genes between H7N9 susceptibility and microbiota features; Table S8: The hub genes ranked by MCC method in PPI network of overlapped genes between H1N1 severity and microbiota features; Table S9: PheWAS results of hub genes in PPI network of overlapped genes between H7N9 susceptibility and microbiota features; Table S10: PheWAS results of hub genes in PPI network of overlapped genes between H1N1 severity and microbiota features; Table S11: Positional mapped genes of 170 IVs for pairs of microbial features and H7N9 susceptibility with significant p value in two-sample MR; Table S12: Positional mapped genes of 232 IVs for pairs of microbial features and H1N1 severity with significant p value in two-sample MR; Table S13: GO pathway enrichment analysis of 216 mapped genes; Table S14: GO pathway enrichment analysis of 304 mapped genes; Table S15: KEGG pathway enrichment analysis of 304 mapped genes.

Author Contributions: Conceptualization, Y.S. and Y.C.; formal analysis, Q.L., F.W., W.Z. and G.L.; methodology, Q.L. and F.W.; writing—original draft preparation, Q.L., F.W. and Y.C.; writing—review and editing, Y.S. and H.Z.; visualization, Q.L. and F.W.; supervision, Y.S. and Y.C. All authors have read and agreed to the published version of the manuscript.

Funding: This research was funded by the National Key Research and Development Program of China, grant number 2021YF C2300100, 2021YF C2300103; the National Natural Science Foundation of China, grant number 82272303 and 81961128002; the Non-profit Central Research Institute Fund of Chinese Academy of Medical Sciences, grant number 2022-RC310-02; the Shenzhen Science and Technology Program, grant number JCYJ20200109142438111; and the Guangdong Provincial Science and Technology Program, grant number 2019B030301009.

Institutional Review Board Statement: The study was approved by the Ethics Committee of the National Institute for Viral Disease Control and Prevention, Chinese Center for Disease Control and Prevention (CDC).

Informed Consent Statement: Written informed consent was obtained from all volunteers. Written informed consent to participate in this study was provided by the participants' legal guardian/next of kin.

Data Availability Statement: The raw data supporting the conclusions of this article will be made available by the authors on request.

Acknowledgments: We thank the China National GeneBank DataBase (CNGBdb); the National Institute for Viral Disease Control and Prevention, Chinese Center for Disease Prevention; the

Chinese National Influenza Surveillance Network; and all staff at local centers for disease control and prevention in China.

Conflicts of Interest: Author Qijun Liao was employed by the company BGI Genomics. The remaining authors declare that the research was conducted in the absence of any commercial or financial relationships that could be construed as a potential conflict of interest.

References

1. Petrova, V.N.; Russell, C.A. The evolution of seasonal influenza viruses. *Nat. Rev. Microbiol.* **2018**, *16*, 47–60. [CrossRef]
2. Li, Y.T.; Linster, M.; Mendenhall, I.H.; Su, Y.C.F.; Smith, G.J.D. Avian influenza viruses in humans: Lessons from past outbreaks. *Br. Med. Bull.* **2019**, *132*, 81–95. [CrossRef]
3. World Health Organization. Influenza (Seasonal). Available online: https://www.who.int/en/news-room/fact-sheets/detail/influenza-(seasonal) (accessed on 3 October 2023).
4. Pinto, R.M.; Bakshi, S.; Lytras, S.; Zakaria, M.K.; Swingler, S.; Worrell, J.C.; Herder, V.; Hargrave, K.E.; Varjak, M.; Cameron-Ruiz, N.; et al. BTN3A3 evasion promotes the zoonotic potential of influenza A viruses. *Nature* **2023**, *619*, 338–347. [CrossRef]
5. Chen, Y.; Graf, L.; Chen, T.; Liao, Q.; Bai, T.; Petric, P.P.; Zhu, W.; Yang, L.; Dong, J.; Lu, J.; et al. Rare variant MX1 alleles increase human susceptibility to zoonotic H7N9 influenza virus. *Science* **2021**, *373*, 918–922. [CrossRef]
6. Everitt, A.R.; Clare, S.; Pertel, T.; John, S.P.; Wash, R.S.; Smith, S.E.; Chin, C.R.; Feeley, E.M.; Sims, J.S.; Adams, D.J.; et al. IFITM3 restricts the morbidity and mortality associated with influenza. *Nature* **2012**, *484*, 519–523. [CrossRef]
7. Ciancanelli, M.J.; Huang, S.X.; Luthra, P.; Garner, H.; Itan, Y.; Volpi, S.; Lafaille, F.G.; Trouillet, C.; Schmolke, M.; Albrecht, R.A.; et al. Infectious disease. Life-threatening influenza and impaired interferon amplification in human IRF7 deficiency. *Science* **2015**, *348*, 448–453. [CrossRef]
8. Brody, H. The gut microbiome. *Nature* **2020**, *577*, S5. [CrossRef]
9. Quan, Y.; Zhang, K.X.; Zhang, H.Y. The gut microbiota links disease to human genome evolution. *Trends Genet.* **2023**, *39*, 451–461. [CrossRef]
10. Chiu, L.; Bazin, T.; Truchetet, M.E.; Schaeverbeke, T.; Delhaes, L.; Pradeu, T. Protective Microbiota: From Localized to Long-Reaching Co-Immunity. *Front. Immunol.* **2017**, *8*, 1678. [CrossRef]
11. Trompette, A.; Gollwitzer, E.S.; Yadava, K.; Sichelstiel, A.K.; Sprenger, N.; Ngom-Bru, C.; Blanchard, C.; Junt, T.; Nicod, L.P.; Harris, N.L.; et al. Gut microbiota metabolism of dietary fiber influences allergic airway disease and hematopoiesis. *Nat. Med.* **2014**, *20*, 159–166. [CrossRef]
12. McAleer, J.P.; Kolls, J.K. Contributions of the intestinal microbiome in lung immunity. *Eur. J. Immunol.* **2018**, *48*, 39–49. [CrossRef]
13. Woodall, C.A.; McGeoch, L.J.; Hay, A.D.; Hammond, A. Respiratory tract infections and gut microbiome modifications: A systematic review. *PLoS ONE* **2022**, *17*, e0262057. [CrossRef]
14. Zhang, Q.; Hu, J.; Feng, J.-W.; Hu, X.-T.; Wang, T.; Gong, W.-X.; Huang, K.; Guo, Y.-X.; Zou, Z.; Lin, X.; et al. Influenza infection elicits an expansion of gut population of endogenous *Bifidobacterium animalis* which protects mice against infection. *Genome Biol.* **2020**, *21*, 99. [CrossRef]
15. Dilantika, C.; Sedyaningsih, E.R.; Kasper, M.R.; Agtini, M.; Listiyaningsih, E.; Uyeki, T.M.; Burgess, T.H.; Blair, P.J.; Putnam, S.D. Influenza virus infection among pediatric patients reporting diarrhea and influenza-like illness. *BMC Infect. Dis.* **2010**, *10*, 3. [CrossRef]
16. Gu, S.; Chen, Y.; Wu, Z.; Chen, Y.; Gao, H.; Lv, L.; Guo, F.; Zhang, X.; Luo, R.; Huang, C.; et al. Alterations of the Gut Microbiota in Patients with Coronavirus Disease 2019 or H1N1 Influenza. *Clin. Infect. Dis.* **2020**, *71*, 2669–2678. [CrossRef]
17. Qin, N.; Zheng, B.; Yao, J.; Guo, L.; Zuo, J.; Wu, L.; Zhou, J.; Liu, L.; Guo, J.; Ni, S.; et al. Influence of H7N9 virus infection and associated treatment on human gut microbiota. *Sci. Rep.* **2015**, *5*, 14771. [CrossRef]
18. Marrella, V.; Nicchiotti, F.; Cassani, B. Microbiota and Immunity during Respiratory Infections: Lung and Gut Affair. *Int. J. Mol. Sci.* **2024**, *25*, 4051. [CrossRef]
19. Davies, N.M.; Holmes, M.V.; Davey Smith, G. Reading Mendelian randomisation studies: A guide, glossary, and checklist for clinicians. *BMJ (Clin. Res. Ed.)* **2018**, *362*, k601. [CrossRef]
20. Chen, H.; Ye, B.; Su, W.; Song, Y.; Sun, P.L.; Zhou, X.; Zhang, G. The causal role of gut microbiota in susceptibility and severity of COVID-19: A bidirectional Mendelian randomization study. *J. Med. Virol.* **2023**, *95*, e28880. [CrossRef]
21. Xu, Q.; Ni, J.J.; Han, B.X.; Yan, S.S.; Wei, X.T.; Feng, G.J.; Zhang, H.; Zhang, L.; Li, B.; Pei, Y.F. Causal Relationship Between Gut Microbiota and Autoimmune Diseases: A Two-Sample Mendelian Randomization Study. *Front. Immunol.* **2021**, *12*, 746998. [CrossRef]
22. Xu, F.; Gan, X.; Tao, Y.; Li, D.; Xie, P.; Liu, F.; Yang, F.; Ma, Y. Association between gut microbiota and influenza: A bidirectional two-sample mendelian randomization study. *BMC Infect. Dis.* **2023**, *23*, 692. [CrossRef]
23. Liu, X.; Tong, X.; Zou, Y.; Lin, X.; Zhao, H.; Tian, L.; Jie, Z.; Wang, Q.; Zhang, Z.; Lu, H.; et al. Mendelian randomization analyses support causal relationships between blood metabolites and the gut microbiome. *Nat. Genet.* **2022**, *54*, 52–61. [CrossRef]
24. Li, M.; Chen, Y.; Chen, T.; Hu, S.; Chen, L.; Shen, L.; Li, F.; Yang, J.; Sun, Y.; Wang, D.; et al. A host-based whole genome sequencing study reveals novel risk loci associated with severity of influenza A(H1N1)pdm09 infection. *Emerg. Microbes Infect.* **2021**, *10*, 123–131. [CrossRef]

25. National Health Commission of the People's Republic of China; National Administration of Traditional Chinese Medicine. Protocol for diagnosis and treatment of influenza (2019 version). *Chin. J. Clin. Infect. Dis.* **2019**, *12*, 451–455.
26. Shang, W.; Zhang, S.; Qian, H.; Pan, X.; Huang, S.; Wen, Z.; Liu, J.; Chen, D. Association of gut microbiota with COVID-19 susceptibility and severity: A two-sample Mendelian randomization study. *J. Med. Virol.* **2023**, *95*, e28734. [CrossRef]
27. Palmer, T.M.; Lawlor, D.A.; Harbord, R.M.; Sheehan, N.A.; Tobias, J.H.; Timpson, N.J.; Davey Smith, G.; Sterne, J.A. Using multiple genetic variants as instrumental variables for modifiable risk factors. *Stat. Methods Med. Res.* **2012**, *21*, 223–242. [CrossRef]
28. Pierce, B.L.; Ahsan, H.; Vanderweele, T.J. Power and instrument strength requirements for Mendelian randomization studies using multiple genetic variants. *Int. J. Epidemiol.* **2011**, *40*, 740–752. [CrossRef]
29. Burgess, S.; Butterworth, A.; Thompson, S.G. Mendelian randomization analysis with multiple genetic variants using summarized data. *Genet. Epidemiol.* **2013**, *37*, 658–665. [CrossRef]
30. Bowden, J.; Davey Smith, G.; Burgess, S. Mendelian randomization with invalid instruments: Effect estimation and bias detection through Egger regression. *Int. J. Epidemiol.* **2015**, *44*, 512–525. [CrossRef]
31. Bowden, J.; Davey Smith, G.; Haycock, P.C.; Burgess, S. Consistent Estimation in Mendelian Randomization with Some Invalid Instruments Using a Weighted Median Estimator. *Genet. Epidemiol.* **2016**, *40*, 304–314. [CrossRef]
32. Burgess, S.; Thompson, S.G. Interpreting findings from Mendelian randomization using the MR-Egger method. *Eur. J. Epidemiol.* **2017**, *32*, 377–389. [CrossRef]
33. Verbanck, M.; Chen, C.Y.; Neale, B.; Do, R. Detection of widespread horizontal pleiotropy in causal relationships inferred from Mendelian randomization between complex traits and diseases. *Nat. Genet.* **2018**, *50*, 693–698. [CrossRef]
34. Cohen, J.F.; Chalumeau, M.; Cohen, R.; Korevaar, D.A.; Khoshnood, B.; Bossuyt, P.M. Cochran's Q test was useful to assess heterogeneity in likelihood ratios in studies of diagnostic accuracy. *J. Clin. Epidemiol.* **2015**, *68*, 299–306. [CrossRef]
35. Wang, K.; Li, M.; Hakonarson, H. ANNOVAR: Functional annotation of genetic variants from high-throughput sequencing data. *Nucleic Acids Res.* **2010**, *38*, e164. [CrossRef]
36. Szklarczyk, D.; Kirsch, R.; Koutrouli, M.; Nastou, K.; Mehryary, F.; Hachilif, R.; Gable, A.L.; Fang, T.; Doncheva, N.T.; Pyysalo, S.; et al. The STRING database in 2023: Protein-protein association networks and functional enrichment analyses for any sequenced genome of interest. *Nucleic Acids Res.* **2023**, *51*, D638–D646. [CrossRef]
37. Malone, J.; Holloway, E.; Adamusiak, T.; Kapushesky, M.; Zheng, J.; Kolesnikov, N.; Zhukova, A.; Brazma, A.; Parkinson, H. Modeling sample variables with an Experimental Factor Ontology. *Bioinformatics* **2010**, *26*, 1112–1118. [CrossRef]
38. Kohler, S.; Gargano, M.; Matentzoglu, N.; Carmody, L.C.; Lewis-Smith, D.; Vasilevsky, N.A.; Danis, D.; Balagura, G.; Baynam, G.; Brower, A.M.; et al. The Human Phenotype Ontology in 2021. *Nucleic Acids Res.* **2021**, *49*, D1207–D1217. [CrossRef]
39. Shannon, P.; Markiel, A.; Ozier, O.; Baliga, N.S.; Wang, J.T.; Ramage, D.; Amin, N.; Schwikowski, B.; Ideker, T. Cytoscape: A software environment for integrated models of biomolecular interaction networks. *Genome Res.* **2003**, *13*, 2498–2504. [CrossRef]
40. Chin, C.H.; Chen, S.H.; Wu, H.H.; Ho, C.W.; Ko, M.T.; Lin, C.Y. cytoHubba: Identifying hub objects and sub-networks from complex interactome. *BMC Syst. Biol.* **2014**, *8* (Suppl. S4), S11. [CrossRef]
41. Watanabe, K.; Stringer, S.; Frei, O.; Umicevic Mirkov, M.; de Leeuw, C.; Polderman, T.J.C.; van der Sluis, S.; Andreassen, O.A.; Neale, B.M.; Posthuma, D. A global overview of pleiotropy and genetic architecture in complex traits. *Nat. Genet.* **2019**, *51*, 1339–1348. [CrossRef]
42. Gene Ontology, C.; Aleksander, S.A.; Balhoff, J.; Carbon, S.; Cherry, J.M.; Drabkin, H.J.; Ebert, D.; Feuermann, M.; Gaudet, P.; Harris, N.L.; et al. The Gene Ontology knowledgebase in 2023. *Genetics* **2023**, *224*, iyad031. [CrossRef]
43. Ashburner, M.; Ball, C.A.; Blake, J.A.; Botstein, D.; Butler, H.; Cherry, J.M.; Davis, A.P.; Dolinski, K.; Dwight, S.S.; Eppig, J.T.; et al. Gene ontology: Tool for the unification of biology. The Gene Ontology Consortium. *Nat. Genet.* **2000**, *25*, 25–29. [CrossRef]
44. Kanehisa, M.; Goto, S. KEGG: Kyoto encyclopedia of genes and genomes. *Nucleic Acids Res.* **2000**, *28*, 27–30. [CrossRef]
45. Sherman, B.T.; Hao, M.; Qiu, J.; Jiao, X.; Baseler, M.W.; Lane, H.C.; Imamichi, T.; Chang, W. DAVID: A web server for functional enrichment analysis and functional annotation of gene lists (2021 update). *Nucleic Acids Res.* **2022**, *50*, W216–W221. [CrossRef]
46. Huang, D.W.; Sherman, B.T.; Lempicki, R.A. Systematic and integrative analysis of large gene lists using DAVID bioinformatics resources. *Nat. Protoc.* **2009**, *4*, 44–57. [CrossRef]
47. Tang, D.; Chen, M.; Huang, X.; Zhang, G.; Zeng, L.; Zhang, G.; Wu, S.; Wang, Y. SRplot: A free online platform for data visualization and graphing. *PLoS ONE* **2023**, *18*, e0294236. [CrossRef]
48. Blander, J.M.; Longman, R.S.; Iliev, I.D.; Sonnenberg, G.F.; Artis, D. Regulation of inflammation by microbiota interactions with the host. *Nat. Immunol.* **2017**, *18*, 851–860. [CrossRef]
49. Budden, K.F.; Gellatly, S.L.; Wood, D.L.; Cooper, M.A.; Morrison, M.; Hugenholtz, P.; Hansbro, P.M. Emerging pathogenic links between microbiota and the gut-lung axis. *Nat. Rev. Microbiol.* **2017**, *15*, 55–63. [CrossRef]
50. Thaiss, C.A.; Zmora, N.; Levy, M.; Elinav, E. The microbiome and innate immunity. *Nature* **2016**, *535*, 65–74. [CrossRef]
51. Ruff, W.E.; Greiling, T.M.; Kriegel, M.A. Host-microbiota interactions in immune-mediated diseases. *Nat. Rev. Microbiol.* **2020**, *18*, 521–538. [CrossRef]
52. Bradley, K.C.; Finsterbusch, K.; Schnepf, D.; Crotta, S.; Llorian, M.; Davidson, S.; Fuchs, S.Y.; Staeheli, P.; Wack, A. Microbiota-Driven Tonic Interferon Signals in Lung Stromal Cells Protect from Influenza Virus Infection. *Cell Rep.* **2019**, *28*, 245–256.e4. [CrossRef]
53. Ichinohe, T.; Pang, I.K.; Kumamoto, Y.; Peaper, D.R.; Ho, J.H.; Murray, T.S.; Iwasaki, A. Microbiota regulates immune defense against respiratory tract influenza A virus infection. *Proc. Natl. Acad. Sci. USA* **2011**, *108*, 5354–5359. [CrossRef]

54. Legoux, F.; Salou, M.; Lantz, O. MAIT Cell Development and Functions: The Microbial Connection. *Immunity* **2020**, *53*, 710–723. [CrossRef]
55. van Wilgenburg, B.; Loh, L.; Chen, Z.; Pediongco, T.J.; Wang, H.; Shi, M.; Zhao, Z.; Koutsakos, M.; Nüssing, S.; Sant, S.; et al. MAIT cells contribute to protection against lethal influenza infection in vivo. *Nat. Commun.* **2018**, *9*, 4706. [CrossRef]
56. Guo, P.; Zhang, K.; Ma, X.; He, P. Clostridium species as probiotics: Potentials and challenges. *J. Anim. Sci. Biotechnol.* **2020**, *11*, 24. [CrossRef]
57. Koh, A.; De Vadder, F.; Kovatcheva-Datchary, P.; Bäckhed, F. From Dietary Fiber to Host Physiology: Short-Chain Fatty Acids as Key Bacterial Metabolites. *Cell* **2016**, *165*, 1332–1345. [CrossRef]
58. Byndloss, M.X.; Olsan, E.E.; Rivera-Chávez, F.; Tiffany, C.R.; Cevallos, S.A.; Lokken, K.L.; Torres, T.P.; Byndloss, A.J.; Faber, F.; Gao, Y.; et al. Microbiota-activated PPAR-γ signaling inhibits dysbiotic Enterobacteriaceae expansion. *Science* **2017**, *357*, 570–575. [CrossRef]
59. Varga, T.; Czimmerer, Z.; Nagy, L. PPARs are a unique set of fatty acid regulated transcription factors controlling both lipid metabolism and inflammation. *Biochim. Biophys. Acta* **2011**, *1812*, 1007–1022. [CrossRef]
60. Alex, S.; Lange, K.; Amolo, T.; Grinstead, J.S.; Haakonsson, A.K.; Szalowska, E.; Koppen, A.; Mudde, K.; Haenen, D.; Al-Lahham, S.; et al. Short-chain fatty acids stimulate angiopoietin-like 4 synthesis in human colon adenocarcinoma cells by activating peroxisome proliferator-activated receptor γ. *Mol. Cell. Biol.* **2013**, *33*, 1303–1316. [CrossRef]
61. Parada Venegas, D.; De la Fuente, M.K.; Landskron, G.; González, M.J.; Quera, R.; Dijkstra, G.; Harmsen, H.J.M.; Faber, K.N.; Hermoso, M.A. Short Chain Fatty Acids (SCFAs)-Mediated Gut Epithelial and Immune Regulation and Its Relevance for Inflammatory Bowel Diseases. *Front. Immunol.* **2019**, *10*, 277. [CrossRef]
62. Antunes, K.H.; Fachi, J.L.; de Paula, R.; da Silva, E.F.; Pral, L.P.; Dos Santos, A.; Dias, G.B.M.; Vargas, J.E.; Puga, R.; Mayer, F.Q.; et al. Microbiota-derived acetate protects against respiratory syncytial virus infection through a GPR43-type 1 interferon response. *Nat. Commun.* **2019**, *10*, 3273. [CrossRef]
63. Park, J.; Kim, M.; Kang, S.G.; Jannasch, A.H.; Cooper, B.; Patterson, J.; Kim, C.H. Short-chain fatty acids induce both effector and regulatory T cells by suppression of histone deacetylases and regulation of the mTOR-S6K pathway. *Mucosal Immunol.* **2015**, *8*, 80–93. [CrossRef]
64. Leylabadlo, H.E.; Ghotaslou, R.; Feizabadi, M.M.; Farajnia, S.; Moaddab, S.Y.; Ganbarov, K.; Khodadadi, E.; Tanomand, A.; Sheykhsaran, E.; Yousefi, B.; et al. The critical role of *Faecalibacterium prausnitzii* in human health: An overview. *Microb. Pathog.* **2020**, *149*, 104344. [CrossRef]
65. Demirci, M.; Tokman, H.B.; Uysal, H.K.; Demiryas, S.; Karakullukcu, A.; Saribas, S.; Cokugras, H.; Kocazeybek, B.S. Reduced *Akkermansia muciniphila* and *Faecalibacterium prausnitzii* levels in the gut microbiota of children with allergic asthma. *Allergol. Immunopathol.* **2019**, *47*, 365–371. [CrossRef]
66. Li, W.; Zhu, Y.; Liao, Q.; Wang, Z.; Wan, C. Characterization of gut microbiota in children with pulmonary tuberculosis. *BMC Pediatr.* **2019**, *19*, 445. [CrossRef]
67. Vernocchi, P.; Del Chierico, F.; Russo, A.; Majo, F.; Rossitto, M.; Valerio, M.; Casadei, L.; La Storia, A.; De Filippis, F.; Rizzo, C.; et al. Gut microbiota signatures in cystic fibrosis: Loss of host CFTR function drives the microbiota enterophenotype. *PLoS ONE* **2018**, *13*, e0208171. [CrossRef]
68. Yeoh, Y.K.; Zuo, T.; Lui, G.C.; Zhang, F.; Liu, Q.; Li, A.Y.; Chung, A.C.; Cheung, C.P.; Tso, E.Y.; Fung, K.S.; et al. Gut microbiota composition reflects disease severity and dysfunctional immune responses in patients with COVID-19. *Gut* **2021**, *70*, 698–706. [CrossRef]
69. Zhou, Y.; Zhang, J.; Zhang, D.; Ma, W.L.; Wang, X. Linking the gut microbiota to persistent symptoms in survivors of COVID-19 after discharge. *J. Microbiol.* **2021**, *59*, 941–948. [CrossRef]
70. Ma, J.; Wu, M.; Wang, Z.; Yang, D.; Hou, S.; Cheng, Y.; Wang, H.; Yan, Y.; Sun, J. Pre-exposure to *Streptococcus suis* improved survival of influenza virus co-infection in mice. *Vet. Microbiol.* **2021**, *258*, 109071. [CrossRef]
71. d'Ettorre, G.; Ceccarelli, G.; Marazzato, M.; Campagna, G.; Pinacchio, C.; Alessandri, F.; Ruberto, F.; Rossi, G.; Celani, L.; Scagnolari, C.; et al. Challenges in the Management of SARS-CoV2 Infection: The Role of Oral Bacteriotherapy as Complementary Therapeutic Strategy to Avoid the Progression of COVID-19. *Front. Med.* **2020**, *7*, 389. [CrossRef]
72. Castelli, V.; d'Angelo, M.; Lombardi, F.; Alfonsetti, M.; Antonosante, A.; Catanesi, M.; Benedetti, E.; Palumbo, P.; Cifone, M.G.; Giordano, A.; et al. Effects of the probiotic formulation SLAB51 in in vitro and in vivo Parkinson's disease models. *Aging* **2020**, *12*, 4641–4659. [CrossRef]
73. Mitchell, J. Streptococcus mitis: Walking the line between commensalism and pathogenesis. *Mol. Oral Microbiol.* **2011**, *26*, 89–98. [CrossRef]
74. Strickland, D.K.; Gonias, S.L.; Argraves, W.S. Diverse roles for the LDL receptor family. *Trends Endocrinol. Metab. TEM* **2002**, *13*, 66–74. [CrossRef]
75. Garcia-Etxebarria, K.; Bracho, M.A.; Galan, J.C.; Pumarola, T.; Castilla, J.; Ortiz de Lejarazu, R.; Rodriguez-Dominguez, M.; Quintela, I.; Bonet, N.; Garcia-Garcera, M.; et al. No Major Host Genetic Risk Factor Contributed to A(H1N1)2009 Influenza Severity. *PLoS ONE* **2015**, *10*, e0135983. [CrossRef]
76. Chin, C.R.; Brass, A.L. A genome wide RNA interference screening method to identify host factors that modulate influenza A virus replication. *Methods* **2013**, *59*, 217–224. [CrossRef]

77. Karlas, A.; Machuy, N.; Shin, Y.; Pleissner, K.P.; Artarini, A.; Heuer, D.; Becker, D.; Khalil, H.; Ogilvie, L.A.; Hess, S.; et al. Genome-wide RNAi screen identifies human host factors crucial for influenza virus replication. *Nature* **2010**, *463*, 818–822. [CrossRef]
78. Uhl, G.R.; Martinez, M.J. PTPRD: Neurobiology, genetics, and initial pharmacology of a pleiotropic contributor to brain phenotypes. *Ann. N. Y Acad. Sci.* **2019**, *1451*, 112–129. [CrossRef]
79. Uhl, G.R.; Martinez, M.J.; Paik, P.; Sulima, A.; Bi, G.H.; Iyer, M.R.; Gardner, E.; Rice, K.C.; Xi, Z.X. Cocaine reward is reduced by decreased expression of receptor-type protein tyrosine phosphatase D (PTPRD) and by a novel PTPRD antagonist. *Proc. Natl. Acad. Sci. USA* **2018**, *115*, 11597–11602. [CrossRef]
80. Tomita, H.; Cornejo, F.; Aranda-Pino, B.; Woodard, C.L.; Rioseco, C.C.; Neel, B.G.; Alvarez, A.R.; Kaplan, D.R.; Miller, F.D.; Cancino, G.I. The Protein Tyrosine Phosphatase Receptor Delta Regulates Developmental Neurogenesis. *Cell Rep.* **2020**, *30*, 215–228.e215. [CrossRef]
81. Huang, X.; Qin, F.; Meng, Q.; Dong, M. Protein tyrosine phosphatase receptor type D (PTPRD)-mediated signaling pathways for the potential treatment of hepatocellular carcinoma: A narrative review. *Ann. Transl. Med.* **2020**, *8*, 1192. [CrossRef]
82. Hsu, H.C.; Lapke, N.; Chen, S.J.; Lu, Y.J.; Jhou, R.S.; Yeh, C.Y.; Tsai, W.S.; Hung, H.Y.; Hsieh, J.C.; Yang, T.S.; et al. PTPRT and PTPRD Deleterious Mutations and Deletion Predict Bevacizumab Resistance in Metastatic Colorectal Cancer Patients. *Cancers* **2018**, *10*, 314. [CrossRef]
83. Ning, H.; Chiu, S.H.; Xu, X.; Ma, Y.; Chen, J.L.; Yang, G. The Immunosuppressive Roles of PD-L1 during Influenza A Virus Infection. *Int. J. Mol. Sci.* **2023**, *24*, 8586. [CrossRef]
84. Julkunen, I.; Sareneva, T.; Pirhonen, J.; Ronni, T.; Melen, K.; Matikainen, S. Molecular pathogenesis of influenza A virus infection and virus-induced regulation of cytokine gene expression. *Cytokine Growth Factor. Rev.* **2001**, *12*, 171–180. [CrossRef]
85. Dejana, E.; Orsenigo, F.; Lampugnani, M.G. The role of adherens junctions and VE-cadherin in the control of vascular permeability. *J. Cell Sci.* **2008**, *121*, 2115–2122. [CrossRef]
86. Jackel, S.; Kiouptsi, K.; Lillich, M.; Hendrikx, T.; Khandagale, A.; Kollar, B.; Hormann, N.; Reiss, C.; Subramaniam, S.; Wilms, E.; et al. Gut microbiota regulate hepatic von Willebrand factor synthesis and arterial thrombus formation via Toll-like receptor-2. *Blood* **2017**, *130*, 542–553. [CrossRef]
87. Hiyoshi, M.; Indalao, I.L.; Yano, M.; Yamane, K.; Takahashi, E.; Kido, H. Influenza A virus infection of vascular endothelial cells induces GSK-3β-mediated β-catenin degradation in adherens junctions, with a resultant increase in membrane permeability. *Arch. Virol.* **2015**, *160*, 225–234. [CrossRef]